

- CCl₄ (Aldrich, 99.9% HPLC grade), which produces HOD by isotopic exchange with trace amounts of H₂O.
21. D. E. Gragson, G. L. Richmond, *J. Phys. Chem. B* **102**, 569 (1998).
 22. J. L. Green, A. R. Lacey, M. G. Sceats, *Chem. Phys. Lett.* **130**, 67 (1986).
 23. J. P. Devlin, *J. Chem. Phys.* **90**, 1322 (1989).
 24. E. Zoidis, J. Yarwood, T. Tassaing, Y. Danten, M. Besnard, *J. Mol. Liq.* **64**, 197 (1995).
 25. T. T. Wall, D. F. Hornig, *J. Chem. Phys.* **43**, 2079 (1965).
 26. The phase of a particular molecular vibration is reflected by the positive/negative sign associated with the amplitude parameter derived from the fitted data.
 27. M. G. Brown, E. A. Raymond, H. C. Allen, L. F. Scatena, G. L. Richmond, *J. Phys. Chem* **104**, 10220 (2000).
 28. J. Lobau, K. Wolfrum, *J. Opt. Soc. Am. B* **14**, 2505 (1997).

29. C. Hirose, N. Akamatsu, K. Domen, *Appl. Spectrosc.* **46**, 1051 (1992).
30. T. Chang, L. X. Dang, *J. Chem. Phys.* **104**, 6772 (1996).
31. The authors gratefully acknowledge NSF (grant CHE-9725751) for support of the liquid/liquid studies; the U.S. Department of Energy, Basic Energy Sciences, for the air/water studies; and the Office of Naval Research for equipment funding.

25 January 2001; accepted 20 March 2001

Controlled Rotation of Optically Trapped Microscopic Particles

L. Paterson,¹ M. P. MacDonald,¹ J. Arlt,¹ W. Sibbett,¹
P. E. Bryant,² K. Dholakia^{1*}

We demonstrate controlled rotation of optically trapped objects in a spiral interference pattern. This pattern is generated by interfering an annular shaped laser beam with a reference beam. Objects are trapped in the spiral arms of the pattern. Changing the optical path length causes this pattern, and thus the trapped objects, to rotate. Structures of silica microspheres, microscopic glass rods, and chromosomes are set into rotation at rates in excess of 5 hertz. This technique does not depend on intrinsic properties of the trapped particle and thus offers important applications in optical and biological micromachines.

Optical forces have been used to trap and manipulate micrometer-sized particles for more than a decade (1). Since it was shown that a single tightly focused laser beam could be used to hold, in three dimensions, a microscopic particle near the focus of the beam, this optical tweezers technique has now become an established tool in biology, enabling a whole host of studies. They can be used to manipulate and study whole cells such as bacterial, fungal, plant, and animal cells (2) or intracellular structures such as chromosomes (3). Optical tweezers make use of the optical gradient force. For particles of higher refractive index than their surrounding medium, the laser beam induces a force attracting the trapped particle into the region of highest light intensity.

The ability to rotate objects offers a new degree of control for microobjects and has important applications in optical micromachines and biotechnology. Various schemes have, therefore, been investigated recently to induce rotation of trapped particles within optical tweezers. This could be used to realize biological machines that could function within living cells or optically driven cogs to drive micromachines.

Besides the use of specially fabricated microobjects (4), two major schemes have successfully enabled trapped microobjects to be set into rotation. The first scheme uses Laguerre-Gaussian (LG) light beams (5–7). These beams have an on-axis phase singularity and are characterized by helical phase fronts (Fig. 1A). The Poynting vector in such beams follows a corkscrewlike path as the beam propagates, and this gives rise to an orbital angular momentum component in the light beam (8). This angular momentum is distinct from any angular momentum due to the polarization state of the light and has a magnitude of $l\hbar$ per photon. Specifically, l refers to the number of complete cycles of phase ($2\pi l$) upon going around the beam circumference. However, to transfer orbital angular momentum to a trapped particle with such a beam, the particle must typically absorb some of the laser light yet still be transparent enough to enable tweezing to occur. This in turn restricts the range of particles to which this method can be applied, and it also further limits this technique because any heating that arises from this absorption could damage the rotating particle. Furthermore, as the particle absorption can be difficult to quantify, controlled rotation of trapped objects in such a beam is very difficult to realize.

The other technique for rotation makes use of the change in polarization state of light upon passage through a birefringent particle (9, 10). For example, circularly polarized light has spin angular momentum

that can be exchanged with a birefringent medium (e.g., calcite) upon propagation of the beam through the medium. This is analogous to Beth's famous experiment—where he measured the torque on a suspended half-wave plate as circularly polarized light passed through it (11)—but here we are working on a microscopic scale. This method has shown rotation rates of a few hundred hertz for irregular samples of crushed calcite, but it is difficult to control and is limited solely to birefringent media so it is not widely applicable. Although both of these methods have proven useful in specific applications, they do have serious shortcomings for general applications in rotating optical microcomponents and realizing optical micromachines.

We introduce a general scheme for rotating trapped microobjects. Specifically, we trap objects within the interference pattern of an LG beam and a plane wave (Fig. 1B) (12). By changing the path length of the interferometer, we are able to cause the spiral

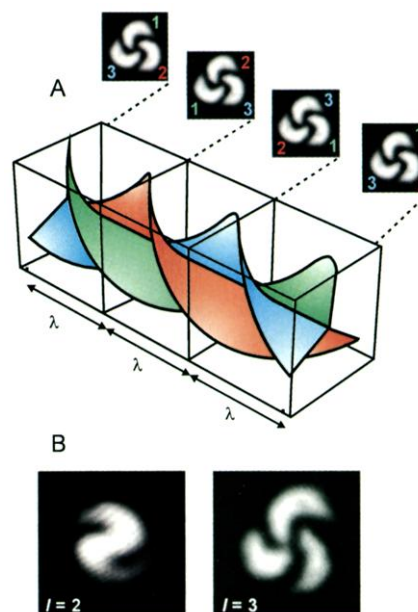


Fig. 1. (A) The phase fronts of an LG beam of azimuthal index $l = 3$ (helical structure) and intensity pattern when interfered with a plane wave. The phase fronts describe a triple start intertwined helix that repeats its shape every λ but only rotates fully after $l\lambda$. In (B), we can see the experimental forms of the interference patterns of LG beams of index $l = 2$ and $l = 3$ with plane waves used in our experiments.

¹School of Physics and Astronomy, St. Andrews University, North Haugh, St. Andrews, Fife KY16 9SS, Scotland. ²School of Biology, Bute Building, St. Andrews University, St. Andrews, Fife KY16 9TS, Scotland.

*To whom correspondence should be addressed. E-mail: kd1@st-and.ac.uk

pattern (and thus the trapped particles) to rotate in a controlled fashion about the axis of the spiral pattern. The rotation of the pattern occurs because of the helical nature of the phase fronts of an LG light beam. A single-ringed LG beam is described by its azimuthal mode index l , which denotes the number of complete cycles of phase upon going around the circumference of the mode. An $l = 2$ or $l = 3$ LG mode (beam) can be thought of as consisting of phase fronts that are double or triple start helices, respectively (see Fig. 1A). Interfering this beam with a plane wave will transform the azimuthal phase variation of the pattern into an azimuthal intensity variation, resulting in a pattern with l spiral arms. As we change the path length in one arm of the interferometer, these spiral arms will rotate around the beam axis. As an analogy, this is akin to considering what occurs along a

length of thick rope that consists of l intertwined cords. Now consider cutting this rope and viewing it end-on. As you move the position of the cut along the rope, any given cord rotates around the rope axis. This is analogous to altering the optical path length in the interferometer. With this technique, we rely solely on the optical gradient force to tweeze trapped particles in the spiral arms and then use the rotation of this spiral pattern under a variation of optical path length to induce particle rotation. The technique can therefore be applied in principle to any object (or group of objects) that can be optically tweezed, in contrast to the other methods listed above. This technique can be extended to the use of LG beams of differing azimuthal index, thus offering the prospect of trapping and rotating different shaped objects and groups of objects. Here, illustrative examples

of rotation with LG beams with azimuthal indices $l = 2$ and $l = 3$ are shown.

Figure 2 shows a schematic of the trapping arrangement (13). A change in the path length in one arm of the interferometer by $l \times \lambda$ will cause a full rotation of 360° of the pattern (and thus the trapped particle array) in the optical tweezers (14). We can readily change the sense of rotation by reducing the path length of one arm of the interferometer instead of increasing it. Thus, in contrast to other rotation methods, we have a very simple way of controlling both the sense and rate of rotation of our optically trapped structure.

The use of an LG $l = 2$ beam results in two spiral arms for our interference pattern, and we used this to rotate silica spheres and glass rods in our tweezers setup (using a $\times 100$ microscope objective). In Fig. 3A, two $1\text{-}\mu\text{m}$ silica spheres are trapped and spun at a rate of 7 Hz. The minimum optical power required to rotate the $1\text{-}\mu\text{m}$ spheres (which is the minimum power required to rotate any of the structures) is 1 mW. Silica spheres coated with streptavidin can bind to biotinylated DNA, and thus one could rotationally orient DNA strands by extending this method. In Fig. 3B, a tweezed glass rod can be seen to rotate between the frames. This constitutes an all-optical microstirrer and has potential application for optically driven micro-machines and motors. We also demonstrate rotation of a Chinese hamster chromosome in our tweezers using this same interference pattern (Fig. 3C), with the axis of our pattern placed over the centromere of the chromosome. This degree of flexibility could be used for suitably orienting the chromosome before, for example, the optical excision of sections for use in polymerase chain reactions. This latter demonstration shows the potential of our method for full rotational control of biological specimens.

The rotation of trapped particles in an interference pattern between an LG ($l = 3$) beam and a plane wave can be seen in Fig. 4. The number of spiral arms in the pattern is equivalent to the azimuthal index of the LG beam used. In this instance, we used a $\times 40$ microscope objective to increase the overall size of the beam profile and thus tweeze and rotate larger structures. In Fig. 4, we see three trapped $5\text{-}\mu\text{m}$ silica spheres rotate in this pattern. One of the spheres has a slight deformity (denoted by the arrow), and the series of pictures charts the progress of this structure of spheres as the pattern is rotated. We typically achieved rotation rates in excess of 5 Hz in the above experiments, which were limited only by the amount of optical power (~ 13 mW) in our interference pattern at the sample plane. The use of optimized components would readily lead to rotation rates of tens to hundreds of hertz. One can envisage other fabricated microobjects being rotated in a similar fashion.

Fig. 2. The experimental arrangement for optical tweezing and subsequent particle rotation in the interference pattern. L, lens; M, mirror; H, hologram; GP, glass plate; BS, beam splitter; Nd:YVO₄, neodymium yttrium vanadate laser at 1064 nm; $\times 100$ or $\times 40$, microscope objectives; CCD, camera; and BG, infrared filter.

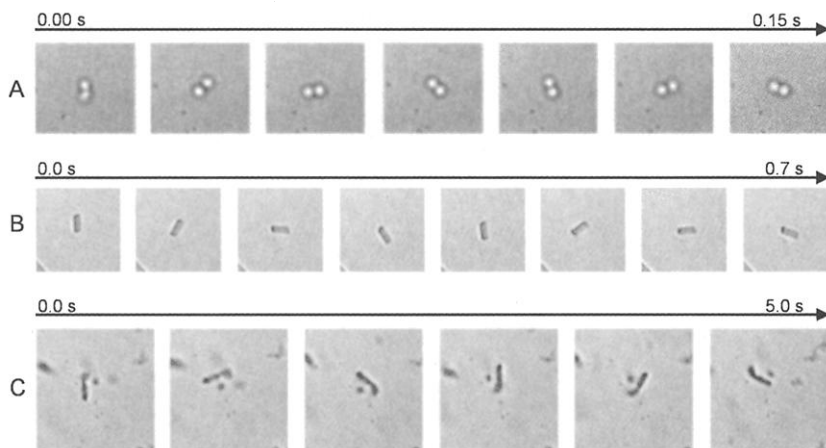
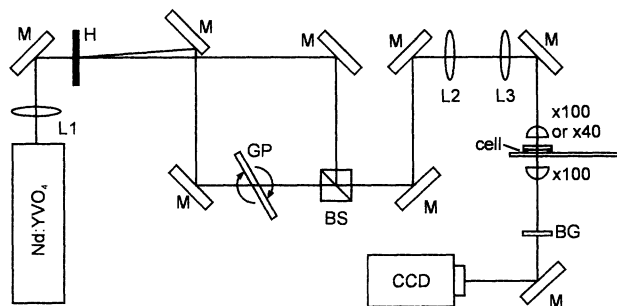
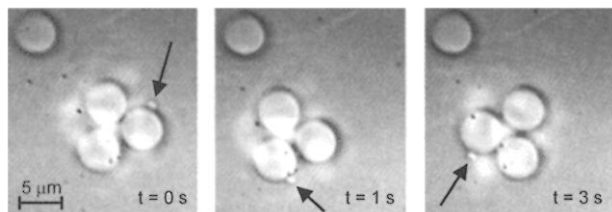


Fig. 3. Rotation of two-dimensionally trapped objects in an LG $l = 2$ interference pattern. (A) Rotation of two trapped $1\text{-}\mu\text{m}$ silica spheres. (B) Rotation of a $5\text{-}\mu\text{m}$ -long glass rod. In (C), we see rotation of a Chinese hamster chromosome. The elapsed time t (in seconds) is indicated by the scale at the top of each sequence of images.

Fig. 4. Rotation of three trapped silica spheres each $5\text{ }\mu\text{m}$ in diameter. The slight deformity (indicated by arrow) on one of the spheres allows us to view the degree of rotation of the structure.



References and Notes

1. A. Ashkin, J. M. Dziedzic, J. E. Bjorkholm, S. Chu, *Opt. Lett.* **11**, 288 (1986).
2. A. Ashkin, J. M. Dziedzic, T. Yamane, *Nature* **330**, 769 (1987).
3. H. Liang, W. H. Wright, S. Cheng, W. He, M. W. Berns, *Exp. Cell Res.* **204**, 110 (1993).
4. P. Ormos, P. Galajda, *Appl. Phys. Lett.* **78**, 249 (2001).
5. H. He, M. E. J. Friese, N. R. Heckenberg, H. Rubinsztein-Dunlop, *Phys. Rev. Lett.* **75**, 826 (1995).
6. M. E. J. Friese, J. Enger, H. Rubinsztein-Dunlop, N. R. Heckenberg, *Phys. Rev. A* **54**, 1593 (1996).
7. N. B. Simpson, K. Dholakia, L. Allen, M. J. Padgett, *Opt. Lett.* **22**, 52 (1997).
8. L. Allen, M. W. Beijersbergen, R. J. C. Spreeuw, J. P. Woerdman, *Phys. Rev. A* **45**, 8185 (1992).
9. M. E. J. Friese, T. A. Nieminen, N. R. Heckenberg, H. Rubinsztein-Dunlop, *Nature* **394**, 348 (1998).
10. M. E. J. Friese, H. Rubinsztein-Dunlop, J. Gold, P. Hagberg, D. Hanstorp, *Appl. Phys. Lett.* **78**, 547 (2001).
11. R. A. Beth, *Phys. Rev.* **50**, 115 (1936).

12. M. Padgett, J. Arlt, N. Simpson, L. Allen, *Am. J. Phys.* **64**, 77 (1996).
13. The experimental setup consisted of a Nd:YVO₄ laser of 300-mW power at 1064 nm. This beam is then directed through an in-house manufactured holographic element (15) that yielded an LG beam in its first order with an efficiency of 30%. This LG beam is then interfered with the zeroth order beam from the hologram to generate our spiral interference pattern. This pattern propagates through our optical system and is directed through either a $\times 40$ or a $\times 100$ microscope objective in a standard optical tweezers geometry. Typically around 1 to 13 mW of laser light was incident on the trapped structure in our optical tweezers, with losses due to optical components and the holographic element. A charge-coupled device (CCD) camera was placed above the dielectric mirror for observation purposes (Fig. 2) when the $\times 100$ objective was used. A similar setup was used when tweezing with a $\times 40$ objective but with the CCD camera placed below the sample slide viewing through a $\times 100$ objective. It is important to ensure

exact overlap of the light beams to guarantee that spiral arms are observed in the interference pattern—at larger angles, linear fringe patterns (with some asymmetry) can result (15). To set trapped structures into rotation, the relative path length between the two arms of the interferometer must be altered. We achieved this by placing a glass plate on a tilt stage in one arm. Simply by tilting this plate, we can rotate accordingly the pattern in the tweezers.

14. The tilting of the glass plate to rotate the interference pattern has a limitation when the plate reaches its maximum angle. One can, however, envisage more advanced implementations for continuous rotation using, for example, a liquid crystal phase modulator in the arm of the interferometer containing the plane wave.
15. M. A. Clifford, J. Arlt, J. Courtial, K. Dholakia, *Opt. Commun.* **156**, 300 (1998).
16. We thank the UK Engineering and Physical Sciences Research Council for supporting our work.

26 December 2000; accepted 19 March 2001

Phonon Density of States of Iron up to 153 Gigapascals

H. K. Mao,¹ J. Xu,¹ V. V. Struzhkin,¹ J. Shu,¹ R. J. Hemley,¹ W. Sturhahn,² M. Y. Hu,² E. E. Alp,² L. Vocadlo,³ D. Alfè,³ G. D. Price,³ M. J. Gillan,³ M. Schwoerer-Böhning,⁴ D. Häusermann,⁴ P. Eng,⁵ G. Shen,⁵ H. Giefers,⁶ R. Lübbers,⁶ G. Wortmann⁶

We report phonon densities of states (DOS) of iron measured by nuclear resonant inelastic x-ray scattering to 153 gigapascals and calculated from ab initio theory. Qualitatively, they are in agreement, but the theory predicts density at higher energies. From the DOS, we derive elastic and thermodynamic parameters of iron, including shear modulus, compressional and shear velocities, heat capacity, entropy, kinetic energy, zero-point energy, and Debye temperature. In comparison to the compressional and shear velocities from the preliminary reference Earth model (PREM) seismic model, our results suggest that Earth's inner core has a mean atomic number equal to or higher than pure iron, which is consistent with an iron-nickel alloy.

The phonon DOS of hexagonal close-packed (hcp) Fe at ultrahigh pressure provides information on the vibrational, elastic, and thermodynamic properties of Fe that are crucial for interpreting seismologic (1, 2) and geomagnetic (3–5) observations deep in the core (6, 7). The full phonon spectrum of Fe has been calculated (8) but needs experimental input for test and improvement. Previous phonon measurements have often been limited to partial phonon information, such as ultrasonic phonon velocities (9), shock-wave velocities (10–12), stress-strain relations (9,

13), and zone-center E_{2g} Raman phonon spectra (14). Nuclear resonant inelastic x-ray scattering (NRIXS), a relatively new tech-

nique (15, 16), has been applied to determine the phonon DOS of body-centered cubic (bcc) Fe at ambient pressure (17) and hcp Fe to 42 GPa (18), but these pressures are still far below the pressure found in the liquid outer core (135 to 330 GPa) and solid inner core (330 to 363 GPa). Moreover, the hcp Fe study also does not yield the correct phonon DOS; i.e., the reported Debye average phonon velocity (V_D) (18) is as much as 20% higher than the ultrasonic and x-ray diffraction results (9). Here we report a new experimental and theoretical comparison. With high-resolution NRIXS measurements, we obtained the phonon DOS of Fe at pressures beyond the core-mantle boundary of Earth. Using ab initio theory, we calculated the phonon DOS and derived elastic and thermodynamic parameters for equivalent pressures. Comparison between experiment and theory provides guidance to the development of the theory for application at the pressure-temperature (P - T) range unattainable by experiments.

In order to achieve core pressures for NRIXS studies and to optimize the detection of the Fe fluorescence (16, 18), we modified

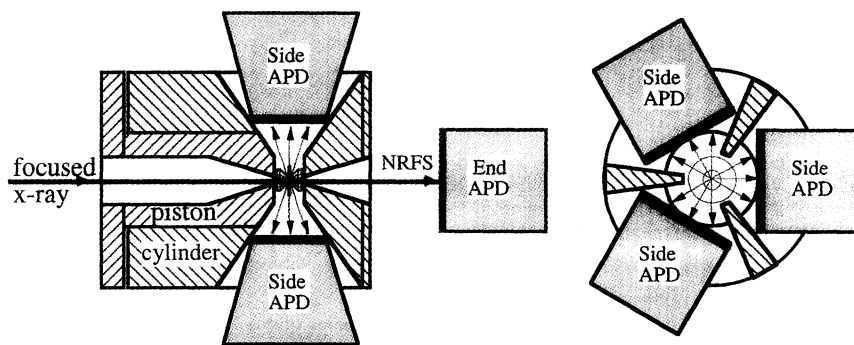


Fig. 1. Wide-angle diamond cell optimized for NRIXS at ultrahigh pressures (left, side view; right, end view). Long piston-cylinder configuration assures the alignment stability critical for reaching ultrahigh pressures. Three windows, each with a 105° equatorial and 68° azimuthal opening [resembling cells developed for neutron diffraction (36)], allow the collection of Fe fluorescence through the high-strength Be gaskets (19) over a huge (40% of the $4\pi r^2$) spherical area by tailor-fitting three APD on the side. The fourth APD at the end records the coherent nuclear forward scattering and monitors the instrument resolution function.

¹Geophysical Laboratory and Center for High Pressure Research, Carnegie Institution of Washington, Washington, DC 20015, USA. ²Advanced Photon Source, Argonne, IL 60439, USA. ³University College London, Gower Street, London WC1E 6BT, UK. ⁴High Pressure Collaborative Access Team (HPCAT), Advanced Photon Source, Argonne, IL 60439, USA. ⁵Consortium for Advanced Radiation Sources, University of Chicago, Chicago, IL 60637. ⁶Fachbereich Physik, University of Paderborn, D33095 Paderborn, Germany.